Hyperglycemia worsens smooth muscle foam cell formation through PI3Kγ-dependent defective autophagy

Labrana H[1*]., Wahart A[1*]., Cormier K[1]., Solinhac R[1]., Swiader A[1]., Mentouri I[1]., Smirnova N[1]., Malet N[1]., Gayral S[1]., Ramel D[1]., Auge N[1]., Laffargue M[1**]**

[1] I2MC, Institut National de la Santé et de la Recherche Médicale (INSERM) U1297, France
***, ** equally contributed**

Authors for correspondence: Muriel Laffargue, PhD or Nathalie Augé, PhD.

Email: muriel.laffargue@inserm.fr, or nathalie.auge@inserm.fr.

ABSTRACT

Diabetic patients are particularly susceptible to cardiovascular complications following atherosclerosis. Uncontrolled glycemia leads to arterial dysfunction, potentially responsible for these increased risks. While the impact of hyperglycemia on endothelial cells and macrophages is well documented, its role in smooth muscle cells (SMCs) remains underexplored. *In vivo*, using a wire injury-based accelerated atherosclerosis mouse model, we showed that hyperglycemia increased lipid loading of SMCs. *In vitro,* we further confirmed this important finding in human primary SMCs exposed to elevated glucose concentrations. This effect originated from a defective autophagy, since autophagy activators prevented lipid droplet accumulation in SMCs. Furthermore, blocking phosphoinositide-3-kinase gamma (PI3Kγ) activity prevented the formation of foam SMCs, by restoring autophagy linked to the nuclear translocation of the transcription factor EB (TFEB), arguing for a major role of this kinase in this process. Understanding the disruption of SMC homeostasis in a hyperglycemic environment holds the promise of a new therapeutic approach, involving PI3Kγ inhibitors, to prevent major cardiovascular diseases (CVD) and their recurrences in diabetic patients.

Introduction

Atherosclerosis is a chronic inflammatory disease that begins with the infiltration of lipids into the arterial intima and culminates with the formation of thrombi, leading to stroke, infarction or ischemia of the lower limbs, depending on the location. The standard treatment for atherosclerosis involves performing angioplasty with stenting to restore arterial blood flow. Despite advancements in patient management, approximately 17.6 % of patients require revascularization within five years of their initial cardiovascular event (Bonaa et al., 2016). Diabetic patients represent a population

at particularly high risk for recurrence (Komaru et al., 2020). Atherosclerosis is notably accelerated in these individuals, leading to the rapid development of complicated plaques. The factors incriminated in this acceleration are dyslipidemia, characterized by elevated levels of atherogenic low-density lipoproteins (LDL), hyperglycemia, oxidative stress and increased inflammation. In particular, hyperglycemia has been proven to exert deleterious effects on endothelial cells, immune cells and smooth muscle cells (SMCs), which are major contributors to the development of atherosclerosis (Poznyak et al., 2020). It has been put forth that hyperglycemia precipitates the dedifferentiation of SMCs (Xi et al., 2019). In their dedifferentiated state, SMCs constitute the predominant cell type in early arterial intimal thickenings and represent an important component of most stages of atherosclerosis (Basatemur et al., 2019). Their remarkable plasticity gives them the ability to take on different phenotypes. Recent single-cell studies have revealed the presence of several subpopulations of synthetic SMCs within human and mouse atherosclerotic plaques, including fibroblast-like cells, chondrocyte-like cells, and cells capable of phagocytosing lipids. These SMC-derived cell phenotypes participate together with macrophages to the pool of intra-plaque foam cells (Bashore et al., 2024; Mocci et al., 2024; Mosquera et al., 2023). Although the proportion of foam cells originating from SMCs *versus* macrophages remains controversial, the existence of these smooth muscle foam cells and their role in atherosclerosis are currently well accepted. Whereas the role of hyperglycemia has been largely studied in macrophages (Qi et al., 2023), whether or not this hyperglycemia could impact foam SMCs has not been clearly investigated.

In order to respond to this significant enquiry, we are utilizing an *in vivo* murine model of hyperglycemia and an *in vitro* model of SMCs exposed to low or high concentrations of glucose. *In vivo*, we demonstrated that hyperglycemia has a specific impact on the SMC lipid loading in intimal hyperplasia induced by an endovascular injury in Western diet-fed LDLR-/- mice. This finding was validated *in vitro* in primary SMCs incubated in high glucose conditions. Furthermore, our findings revealed that this effect was attributable to a reduction in autophagy, induced by high concentrations of glucose and could be reversed by autophagy activators. We then demonstrated an unanticipated role of the specific PI3Kγ isoform in these processes through the regulation of TFEB, a transcription factor governing autophagy. Finally, inhibiting PI3Kγ proved effective in restoring a normal autophagic flux and blocking the development of foam SMCs.

Materials and Methods

Availability of Data and Materials: Upon reasonable request to the corresponding authors, the data and materials supporting the findings of this study are available.

Antibodies

The rabbit anti-α-SMA polyclonal antibody (#RB9010P1) was purchased from Epredia. The rabbit anti-LC3 polyclonal antibody (#2775), the rabbit phospho-TFEB (S211) monoclonal antibody (#37681), the rabbit anti-GAPDH monoclonal antibody (#2118), the anti-mouse IgG HRP-linked (#7076), and the anti-rabbit HRP-linked antibodies (#7074) were purchased at Cell Signaling Technology. Rabbit polyclonal TFEB antibodies used for immunofluorescence (#A303-673A) and Western Blot analysis (#13372-1-AP) were bought at Bethyl Laboratories and Proteintech respectively. The mouse anti-histone deacetylase 1 (HDAC1) monoclonal antibody (sc-8410) was purchased at Santa Cruz Biotechnology, Inc. The immunofluorescence analysis secondary antibodies AlexaFluor488 goat anti-rabbit (#A11008), and AlexaFluor555 goat anti-rabbit (#A32732) were purchased at Invitrogen.

Other materials and Reagents

Dulbecco's Modified Eagle Medium, no glucose (DMEM, 11966-025), Fœtal Bovine Serum (FBS, A31608-01) and Opti-MEM (31985-047) were purchased from Gibco. D-Glucose (G7021), Streptozotocin (S0130), Rapamycin (R0395), LY294002 (L9908), XtremeGENE 9 DNA (6365787001), Nile Red (N-3013) DAPI (D9542) and Bafilomycin (B1793) were purchased from Sigma-Aldrich and NBD-cholesterol (N1148) from Life Technologies. BSA (04-100-812C) was from Euromedex and 3-MethylAdenine (HY-19312) from Clinisciences. A66 (S2636), AZD 6482 (S1462) and IPI-549 (S8330) were obtained from SelleckChem. DiIC_{18} 1,1'dioctadecyl-3,3,3',3'tetrametyl-indocarbocyanine perchlorate (D3911), Lipofectamine 2000 (H668-019) and Bodipy 493/503 (D3922) were purchased from Invitrogen.

Animals studies

Male C57Bl/6J LDL receptor-deficient (LDLR$^{-/-}$) mice and male Wild-Type C57BL/6J (WT) mice were obtained from Charles River Laboratories (Wilmington, MA, USA) and ENVIGO (Gannat) respectively. Male PI3Kγ-deficient (PI3Kγ KO) mice were from a C57BL/6J background and have been described earlier (Hirsch et al., 2000). All mice were maintained in specific opportunist and pathogen-free conditions at the CREFRE

breeding facility (US006, Toulouse, France) and used in accordance with institutional guidelines from Directive 2010/63/EU of the European Parliament or the NIH guidelines for the protection of animals used for scientific purposes.

For the injury-induced atheromatous protocol, eight-weeks-old LDLR$^{-/-}$ male mice were fed with Western diet (42% from fat, 0,2% cholesterol, MD.88137, ENVIGO) for 9 weeks. After 2 weeks of dietary adaptation, mice were randomly assigned to receive low doses of streptozotocin (50 mg/kg, STZ group) or vehicle (Control group) for 5 days. Then, mice underwent carotid artery surgery and were euthanized 4 weeks later for blood and tissue collection.

Carotid Artery Wire Injury

Endovascular injury of the carotid artery was performed as previously described (Lupieri et al., 2020). Briefly, mice were anaesthetized with an intraperitoneal injection of a ketamine (100 mg/kg)/xylazine (20 mg/kg) mix followed by a buprenorphine injection (100 µg/kg). The left common carotid artery was isolated and the external carotid incised under a surgical stereomicroscope (Carl Zeiss). A 0.35-mm diameter angioplasty guidewire (Abbott Vascular) was introduced into the artery and withdrawn three times (5 mm length in total) to induce de-endothelialization. The external carotid artery was ligated, post-wire removal, restoring blood flow to the common and left carotid artery. After 4 weeks, the injured carotid arteries were collected for subsequent immunofluorescence analysis.

Tissue Processing and Lesion Analysis

Injured carotids were frozen on a cryostat mount with optimum cutting temperature (n°4583; Tissue-Teck) and sectioned into 10 µm segments from the common carotid over the length of 250 µm using a cryostat microtome (Cryostar NX50, Microm Microtech). Sections were washed with PBS (Phosphate-Buffered Saline), fixed with 4% paraformaldehyde in PBS (PFA) and permeabilized with 0.1% of Triton X-100 in PBS and blocked with 3% bovine serum albumin (BSA) in 0.1% Triton in PBS for 1h. Subsequently, primary antibody was applied and incubated overnight at 4°C. Following secondary antibody incubation, neutral lipids were stained with Bodipy 493/503 (1:1000) for 30 min and nuclei were counterstained with DAPI (100µg/mL for 5 min at room temperature (RT).

Cell Culture

Human SMCs were isolated from mesenteric arteries of deceased anonymous donors (Swiader et al., 2016). SMCs were isolated from three different mesenteries (anonymous N° 75224, 89049 and 92224) and were immortalized (hSMC) by transfection of SV40T antigen, using Lipofectamine LTX Reagent and Plus Reagent (Invitrogen/Life Technologies). Cells were routinely maintained in DMEM, 10% foetal bovine serum (FBS) supplemented with 1 g/L glucose, at 37°C in a humidified 5% CO_2 air atmosphere. Experiments were realised with cells from passages 4 to 20. Mouse SMCs were isolated from WT and PI3Kγ KO mice according to a modified protocol described by Ray et al. (Ray et al., 2001). In brief, aortae from 10 WT and 10 PI3Kγ KO mice were dissected from their origin to the iliac bifurcation, flushed with PBS, and removed. The adventitia was removed from the aortae and the smooth tubes were cut into pieces of 1–2 mm, and then digested in 0.3% collagenase solution. Collagenase digestion was stopped by adding DMEM/10% FBS. Then, the pieces of aortae were washed twice and seeded in culture dishes coated with 10 µg/ml human fibronectin (BD Biosciences). Primary confluent cultures were trypsinized at 37°C, and then cells were incubated at 37°C in 5% CO_2 in DMEM/10% FBS.

si-RNA transfection

SMCs were transfected using Lipofectamine 2000, according to the manufacturer's protocol. si-RNA sequences were purchased at Qiagen. The two target sequences of si-RNA against Atg5 were as follows: TCCAACTTGTTTCACGCTATA (SI00069251) and AACCTTTGGCCTAAGAAGAAA (SI022655310). The two target sequences against Atg7 were: ATCAGTGGATCTAAATCTCAA (SI02655373) and ATCGGATGAATGAGCCTCCAA (SI04231360). Target sequences against TFEB were: GAGACGAAGGTTCAACATCAA (SI00094976) and CACAGGCTGTTGTGAGGACTA (SI04384240). For each experiment a comparison with a negative siRNA was performed (Cat. No.:1027281). The silencing efficiency was measured by Real-time PCR analysis.

LDL Isolation and Oxidation

Human LDL and HDL (High-density lipoprotein) were isolated from pooled fresh sera by sequential ultracentrifugations, dialyzed and sterilized by filtration. LDL oxidation by UV-C irradiation was obtained as previously described (Auge et al., 2004). ApoA-1 was prepared from HDL as described before (Osborne, 1986).

Cellular immunofluorescence

After stimulation, the cells plated onto a cover glass were rinsed with PBS, fixed with 4% PFA, and blocked for 30 min in 3% BSA in PBS. Cells were incubated, 1 h with primary antibodies (1:100) and after rinsing, 1 h with Alexa fluor secondary antibodies (1:500). Neutral lipids and nuclei were stained as described above. Microscopy imaging was performed using a Zeiss LSM780 confocal microscope equipped with a Plan Apochromat 40× 1.20 NA water-immersion objective lens and a Plan Apochromat 63× 1.4 NA oil-immersion objective lens. Lesion characterization and cell images were analysed using ImageJ software.

Autophagic flux

SMCs cultured in 1 g/L or 5 g/L during 10 days were transfected with pcDNA3-GFP-LC3-RFP-LC3ΔG construct (Addgene, 168997 deposited by Noboru Mizushima) as described previously (Kaizuka et al., 2016) using the manufacturer's protocol of XtremGENE 9 DNA transfection agent. 24 hours after transfection cells were washed and then fixed with 4% PFA in PBS for 15 min at RT. Nuclei were labelled with DAPI, 5 min at RT. Images were captured by LSM780 confocal microscope equipped with a Plan Apochromat 63× 1.4 NA oil-immersion objective lens. Fluorescence analysis were performed using ImageJ software and data from each condition were represented as the ratio of median GFP fluorescence to RFP fluorescence.

Foam Cell Formation Assay

Foam cell formation was quantified after cell fixation and permeabilization (as described for cellular immunofluorescence) by Nile Red (1:1000, 3 min) or Bodipy 493/503 (1:1000, 30 min) staining and DAPI counterstaining (1 µg/mL in PBS). Staining was assessed by fluorescence microscopy (ZOE™, Biorad) and quantified after fluorescence eluting with NaOH solution (0,3 M) at 37°C (for Bodipy λ_{ex}: 485 nm-λ_{em}:535nm/ for nile red λ_{ex}: 591nm-λ_{em}: 657nm, normalized to nucleus labeling). Alternatively, intracellular total and esterified cholesterol levels were quantified using a cholesterol fluorometric assay kit (Abcam, ab65359). The level of intracellular cholesterol was normalized to the protein concentration of the sample.

Oxidized LDL uptake assay

SMCs cultured in 1 g/L and 5 g/L 10%FBS/DMEM medium for 7 days were passaged and incubated in 1 g/L and 5 g/L 1%FBS/DMEM medium, supplemented with carbocyanine-

oxLDL (60 µg/mL) and oxLDL (100 µg/mL) for 24 hours (Di-oxL). After treatment, cells were fixed using 4% PFA in PBS, permeabilized with Triton X-100 0.1% in PBS and nuclei were counterstained with DAPI 5 min at RT. Images were captured using fluorescent microscopy (ZOE, Biorad) and then quantified after fluorescence eluting with NaOH solution (0,3 M) at 37°C (λ_{ex}: 530nm-λ_{em}: 580nm normalized to nucleus labeling).

Cholesterol efflux assay

After 7 days in 10%FBS/DMEM at 1 g/L or 5 g/L glucose, cells were passaged in 1%FBS/DMEM medium and loaded with 1 µg/mL NBD-cholesterol for 48 hours. Then, SMCs were rinsed with PBS and equilibrated in DMEM without phenol red/0,5% BSA medium for 2h, and incubated in 1 g/L and 5 g/L glucose 1% FBS/DMEM medium without phenol red containing ApoA-1 (100 µg/mL) and HDL (100 µg/mL) and 1 or 5 g/L glucose for 24 hours. Next, the medium was collected, and the cells were lysed at 37°C with 0.3 M NaOH solution. The fluorescence intensity was measured in both fraction with a TECAN microplate spectrophotometer (λ_{ex}: 485 nm-λ_{em}:535nm). Efflux was calculated as follows: Efflux = $NBD_{fluorescence}$ in medium / ($NBD_{fluorescence}$ in medium + $NBD_{fluorescence}$ in cell lysate). Displayed values represent subtracting effluxes of the wells without apoA-I or HDL from those containing apoA-I or HDL.

Western Blot analysis

Cell extracts were prepared using RIPA lysis buffer supplemented with protease/phosphataseinhibitors. Nuclear/cytosolic extract were obtained using the NE-PER Nuclear and cytoplasmic extraction reagents (#78835, Thermo Fisher Scientific) following manufacturer protocol. Protein levels were assessed byBradford assay. For regular western, equal amount of protein samples was separated by SDS-PAGE. Nonspecific binding was blocked with 5% BSA in Tris buffer saline (TBS) for 2h at RT. Blots were incubated overnight at 4°C with following primary antibodies: anti-LC3 (1:1000), anti-TFEB (1 :1000), anti P-TFEB (S211) (1:1000). β-actin and α-tubulin were used as loading control. After 3 washes with Tris Buffered Saline (TBS) 0,1%Tween20, membranes were incubated with secondary antibodies for 1h at RT. Membranes were scanned using Chemidoc Touch imaging system (Biorad) and proteins were detected by ECL reagents. The bands intensities were quantified using ImageJ software.

Real-time quantitative PCR

Total RNA was extracted from VSMCs using Trizol reagent and cDNA was amplified using a High-Capacity cDNA Reverse Transcription Kit (Thermo Fisher Scientific,

4368813) on a thermocycler (T100 Biorad #1861096). Real time quantitative PCR was performed using StepOnePlus Real Time PCR System and the results were analyzed using StepOne Software v2.3. The primers for the HPRT were 5'-TTGCTCGAGATGTGATGAAGGA−3' (forward) and 5'- CCAGCAGGTCAGCAAAGAATT −3' (reverse). The primers for human ABCA1 were 5'- CACCCCGTATGAACAGGATT-3' (forward) and 5'- GCCAAGGACCAAAGTGATG-3' (reverse). The primers for human ABCG1 were 5'-ATTCAGGGACCTTTCCTATTCGG-3' (forward) and 5'-CTCACCACTATTGAACTTCCCG-3' (reverse). The primers for the human LC3 receptor were 5'- AGCAGCTTCCTGTTCTGGAT−3' (forward) and 5'-TGAGCTGTAAGCGCCTTCTAA −3' (reverse). The primers for human LAMP-1 were 5'-TCCAGGCGTACCTTTCCAACAG −3' (forward) and 5'-TGTCTTGTTCACAGCGTGTCTCTC −3' (reverse). The primers for human Atg5 were 5'-TGGATTTCGTTATATCCCCTTTAG−3' (forward) and 5'- CCTAGTGTGTGCAACTGTCCA −3' (reverse). The primers for Atg7 were 5'- CCGTGGAATTGATGGTATCTGT −3' (forward) and 5'-TCATCCGATCGTCACTGCT −3' (reverse). The primers for human TFEB were 5'- CCATCACCTGGACTTCAGCC−3' (forward) and 5'-CTTGGACAGGCTGGGGAATG −3' (reverse). The primers for murine LC3 were 5'-ATTGCTGTCCCGAATGTCTC' (forward) and 5'- CGTCCTGGACAAGACCAAGT −3' (reverse). The primers for murine LAMP-1 were 5'- GCAACTTCAGCAAGGAAGAGAC−3' (forward) and 5'- AACATTGTACTTGGATACAGTGGG −3' (reverse) and for murine HPRT CCTCCTCAGACCGCTTTTT (forward) and AACCTGGTTCATCATCGCTAA (reverse). The 2ΔΔCt method was used to calculate the fold changes in gene expression. HPRT served as the control for comparison. qRT-PCR was performed in triplicate and repeated in at least three separate experiments.

Statistical Analysis

Data are presented as the mean ± standard error of measurement (SEM) of 3 to 8 independent experiments. The statistical analysis procedure was defined after performing a normality test (Shapiro-Wilk) to ensure equality of variances. To compare two experimental conditions, the results were analysed using Student's parametric test or the non-parametric Wilcoxon or Mann Whitney tests, when the variances were equal or unequal respectively. Beyond 3 experiments, the data were compared using parametric two-factor ANOVA or non-parametric Friedman's test, for equal or unequal variances respectively. Statistical analyses were performed using Prism 10 software (GraphPad software). Results were considered statistically significant when $p<0.05$.

Results

High glucose concentration enhances lipid accumulation in smooth muscle cells *in vitro* and *in vivo*

To investigate the impact of hyperglycemia on atherosclerosic lesions, we developed a wire injury-based model of accelerated atherosclerosis in hyperglycemic mice. Briefly, an endovascular injury of the carotid artery was performed (Lupieri et al., 2020) in western diet-fed LDLR$^{-/-}$ mice rendered hyperglycemic or normoglycemic respectively by repeated injections of low doses of streptozotocin (STZ) or vehicle (Ctrl) (Figure 1A). As expected, STZ-treated mice showed a significant increase in blood glucose levels after 7 days (325+/- 40.9 mg/dL *vs* 173.6+/- 9.7 mg/dL in Ctrl mice, ***$p<0.001$) and reached 514.5+/- 57.2 mg/dL at the end of the protocol (Table 1). One month after the carotid artery injury, both groups of mice (Ctrl and STZ) developed a lipid-rich neointima at the lesion site, mainly composed of SMCs as revealed by α-SMA labelling (Figure 1B-D). Despite a non-significant increase in the total lipidic area, lesions from STZ-treated mice exhibited a significant increase in colocalization of α-SMA with bodipy labeling (Pearson correlation coefficient) of 0.443+/-0.0375 *vs* 0.251+/-0.0.22 in ctrl mice, ** $p< 0.01$, Figure1D). These data suggest that STZ treatment led to increased foam SMC content in the neointima of atherosclerosis-prone injured arteries. Analysis of the blood metabolic profile of these mice revealed that despite a significant increase in plasmatic LDL, STZ-treated mice had an unchanged LDL/HDL ratio (Table 1). To further investigate the possible direct impact of hyperglycemia on foam SMC formation, we cultured human and mouse SMCs with low (L, 1 g/L) or high (H, 5 g/L) glucose concentration. After incubation of SMCs with oxidized low-density lipoprotein (OxL), we observed a dramatic increase in intracellular lipid accumulation in high glucose compared to low glucose condition in both human and mouse cells (Figure 1E, F respectively). Consistent with these changes, the total intracellular cholesterol, especially cholesterol ester rates, were also increased under elevated glucose concentration in human SMCs (Suppl. Fig. 1A, B). Altogether, our results demonstrate that high glucose concentration favours SMC-derived foam cell accumulation *in vivo* and *in vitro*.

As the formation of foam cells is associated with either altered OxLDL uptake and/or impaired cholesterol efflux (Xue et al., 2010), we analysed both mechanisms under elevated glucose concentration. Our analysis showed that after short exposures to OxLDL, no difference was observed in the intracellular accumulation of these

lipoproteins in the presence of different concentrations of glucose, suggesting that SMC lipid accumulation is affected by high glucose concentration beyond the process of OxLDL uptake (Suppl. Fig. 1C). Consistently, SMCs cultured with a high glucose concentration demonstrated reduced free cholesterol efflux by more than 72 % and 35 % towards ApoA and HDL respectively compared to low glucose concentration (Suppl. Fig. 1D). Moreover, while the addition of OxLDL to the medium induced a significant increase in ATP-binding cassette A1 (ABCA1) and ATP-binding cassette G1 (ABCG1) transporter gene expression in SMCs, high glucose concentration did not affect this process (Suppl. Fig. 1E, F). Altogether, these results indicated that high glucose concentration leads to an impairment in lipid degradation by SMCs.

High glucose concentration-induced lipid accumulation in SMCs is due to defective autophagy

Current literature suggests that lipid degradation occurs through an autophagy-related process in macrophages and SMCs (Robichaud et al., 2022). To investigate if elevated glucose concentrations could affect this process, we assessed LC3I/II expression in SMCs cultured in both glucose concentrations. Chronic incubation with high glucose concentration led to a 50 % decrease in LC3-II protein expression compared to low-rate glucose exposition and this was independent of a 3 day-treatment with OxLDL (Figure 2A and Supp. Fig. 2). Moreover, LC3-II expression in the presence of autophagy poison (Bafilomycin A), showed a dramatic decrease of the autophagy flux in the presence of high glucose concentration (Figure 2A, B). Analysis of the GFP-LC3- RFP-LC3ΔG probe evolution in these cells strengthened our observations as GFP/RFP ratio was significantly increased when cells were incubated with high glucose concentrations (Figure 2C).

To confirm the causal role of autophagy regulation in high glucose-induced foam SMC formation, we assessed the effects of genetical or pharmacological autophagy modulation in both low and high glucose conditions. First, ATG5 (autophagy related gene 5) and ATG7 (autophagy related gene 7) were knocked down by si-RNA to effectively abolish the autophagic process by limiting the expression of its partners (Figure 2D). ATG5 and ATG7 deficiency promoted foam cell formation in low glucose condition, without interfering with the effects observed when cells are cultured with high glucose concentration (L/ATG5 2.01±0.4, H/ATG5 1.8±0.2, *p<0.05, Figure 2E). These findings were further confirmed by the use of 3-methyladenine (3Ma), a specific autophagy inhibitor, that induced a two-fold increase in foam cell formation with low but not high glucose concentration (Figure 2F). A two-fold accumulation of total

cholesterol in SMCs, especially cholesterol esters, and an 80 % decrease of cholesterol efflux towards ApoA were also observed in the presence of 3Ma in low glucose concentration (Supp. Fig. 3A-C). In contrast, the addition of the mTORC1 inhibitor rapamycin (Rp), a potent autophagy activator, significantly protected SMCs from high glucose-induced lipid accumulation, and attenuated foam cell formation (H/Rp(-) 3.1±0.5, H/Rp(+) 0.7±0.1, *p<0.05, Figure 2G). Consistent with these results, Rp treatment also limited the total cholesterol and cholesterol ester accumulation, along with the recovery of the cholesterol efflux to ApoA (Supp. Fig. 3D-F). Together, these findings confirmed that the downregulation of autophagy by high glucose is responsible for increased foam cell formation.

PI3Kγ drives increased foam SMC formation under high glucose concentration

We aimed at deciphering the molecular mechanism underlying the effects of high glucose. The PI3K/Akt/mTOR pathway is largely involved in autophagy regulation in vascular foam SMCs (Pi et al., 2021). Using the pan-PI3K inhibitor LY294002 we confirmed that PI3K activity is involved in high glucose-induced foam SMC formation (Figure 3A). Nevertheless, the exact isoform of PI3K, involved in this process under high glucose conditions still needed to be identified. We therefore used specific PI3K isoform inhibitors against PI3Kα (A66), PI3Kβ (AZD-6482) and PI3Kγ (IPI-549) on SMCs cultured with low or high glucose concentrations. We found that the PI3Kγ inhibitor IPI-549 was the most effective at preventing foam SMC formation induced by high glucose (Figure 3B). Accordingly, in high glucose conditions, IPI-549 markedly decreased intracellular total cholesterol content and restored free cholesterol generation to the same level as those observed in SMCs in low glucose concentration (Figure 3C). In addition, IPI-549 restored 80 % of the efflux to ApoA (Figure 3D). Finally, to confirm the involvement of PI3Kγ in these processes, we performed the same experiments in primary SMCs obtained from WT or PI3KγKO mice. In murine cells, genetic invalidation of PI3Kγ (Figure 3E) prevented high glucose-induced foam SMC formation. Altogether, these data identified PI3Kγ as a specific regulator of high glucose-dependent foam SMC formation.

Blocking PI3Kγ reverses high glucose-induced autophagy alterations by modulating the nuclear translocation of TFEB

To further decipher how PI3Kγ inhibition counteracted foam SMC formation, we analysed autophagy dynamics in both human and murine SMCs (hSMC and mSMC). In hSMCs, pharmacological inhibition of PI3Kγ led to an increase in LC3 staining (Figure

4A) in high glucose. Moreover, the expression of autophagy-related genes, lysosomal-associated membrane protein 1 (LAMP-1 and LC3, reduced by 35% in high glucose condition, was restored by IPI-549 (Figure 4B). Consistently, genetic invalidation of PI3Kγ in mSMCs did not impact LC3 expression in high glucose compared to low glucose condition (Figure 4C). Autophagic flux assays were carried out on mSMCs, pre-treated with low or high glucose medium, using the GFP-LC3-RFP-LC3ΔG probe. As observed in Fig. 4D, the GFP/RFP ratio observed in high glucose is higher in WT SMCs in comparison to PI3Kγ-KO SMCs, meaning a higher autophagic flux when PI3Kγ is not functional (Figure 4D). Moreover, high glucose significantly decreased LAMP-1 and LC3 gene expression by 40 % and 30 % respectively, in murine WT SMCs compared to low glucose medium (Figure 4E). Interestingly, the lack of PI3Kγ in high glucose condition maintained autophagy gene expression at the same levels as in low glucose condition (Figure 4F). Collectively, our data demonstrate that specific modulation of PI3Kγ activity in high glucose conditions is sufficient to restore the autophagic process in SMCs. To delineate the molecular mechanisms linking PI3Kγ to the regulation of autophagy, we investigated the involvement of TFEB, a master transcriptional regulator of autophagy: indeed, nuclear translocation of TFEB induces the transcription of key autophagy genes, and can be regulated through PI3K/mTOR pathway (Napolitano and Ballabio, 2016). Genetic knockdown of TFEB enhanced foam cell formation under low-glucose conditions without affecting high-glucose conditions despite an effective reduction in TFEB expression in both conditions (Figure 5A, B). Furthermore, TFEB downregulation led to decreased LAMP-1 and LC3 gene expression in cells cultured under low but not high glucose conditions, suggesting a key role of this transcription factor in high glucose-induced defective autophagy (Figure 5C, 5D). Western blot analysis revealed a significant decrease in TFEB nuclear translocation in SMCs cultured in high glucose compared with the low glucose condition (Figure 5E, 5F). Additionally, chronic exposition of SMCs to high glucose induced the phosphorylation of TFEB on Serine 211, suggesting that TFEB in the cytosol (Figure 5G). Incubation of SMCs with the PI3Kγ specific inhibitor IPI-549 significantly reduced S211-TFEB phosphorylation induced by high glucose (Figure 5G). Consistently, IPI-549 rescued the nuclear translocation of TFEB, that was impaired by high glucose concentration (H/IPI-549 (-) 0.24±0.1, H/IPI-549(+) 0.63±0.23, *p<0.05, Figure 5H).

Thus, the inhibition of PI3Kγ induces a desensitization of SMCs to high glucose-impaired autophagy, through the recovery of TFEB nuclear translocation, enabling the subsequent expression of autophagy key genes.

Discussion

Our results demonstrate that hyperglycemia promotes *in vivo* and *in vitro* SMC-derived foam cell formation. Using a wire injury-based model of accelerated atherosclerosis in hyperglycemic mice, we demonstrated that hyperglycemia led to lesions enriched in foam SMCs compared to normoglycemic mice. Previous studies in the literature demonstrated the impact of hyperglycemia on the acceleration of atherosclerotic plaque formation in the aortic sinus using ApoE$^{-/-}$ mice rendered diabetic with streptozotocin (Gistera et al., 2022). However, the role of SMCs in this context remained unclear. Our model, which uses a guidewire to denude the endothelium, has the peculiarity of a rapidly developing atherosclerosis characterized by a massive lipid infiltration in SMA-positive SMCs. This model has allowed us to demonstrate for the first time that elevated blood glucose levels have a deleterious effect on SMCs under atheromatous conditions by promoting their intracellular lipid accumulation.

In vitro, SMCs chronically exposed to high glucose medium in the presence of oxLDL significantly increase neutral lipid engulfment in comparison with low glucose condition. Our results, unlike the work of Xue and al., demonstrate that high glucose concentration did not induce any modification of LDL uptake nor decrease of cholesterol efflux receptor expression (Xue et al., 2010). Indeed, while they reported a reduction of ABCG1 expression in SMCs cultured in oxLDL- and high glucose-enriched medium, our work rather shows that high glucose alone induces an alteration in autophagy. In the literature, lipid-associated autophagy is referred to as lipophagy (Liu and Czaja, 2013). Our results therefore suggest that high glucose concentrations are capable of modifying this specific lipophagy mechanism.

In our study, high glucose concentration-impaired autophagy is due to the alteration of key autophagy key gene expression. Interestingly, these detrimental effects have been found in the monolayer of the vascular wall from gestational and type 2 diabetes mellitus patients, supporting a defective autophagic activation in diabetic conditions (Chen et al., 2024; Xu et al., 2024; Zhao et al., 2022). Accordingly, we found that elevated glucose concentrations reduced autophagy process through TFEB nuclear translocation impairment, reinforcing the role of TFEB in autophagy regulation in SMCs, as it has been proposed by Chen and al. (Chen et al., 2022).

Foam SMC formation has been associated with the PI3K class I pathway (Pi et al., 2021). Here we demonstrate an unexpected role of the gamma isoform of the PI3K family in response to high glucose in SMC foam cells. In foam macrophages, the role of the gamma isoform has been suggested but not clearly demonstrated (Anzinger et al., 2012; Michael et al., 2015). Chang and al. showed that in PI3Kγ-deficient mice, foam

macrophage formation is reduced. This phenomenon likely originates from an indirect inhibitory effect on inflammation, resulting in a decreased foam cell content inside the plaque (Chang et al., 2007). Here, we identify for the first time that in high glucose concentration, PI3Kγ controls TFEB phosphorylation leading to decreased autophagy and lipid accumulation. These data suggest that elevated glucose concentrations potentiate PI3Kγ activity. One possible mechanism could be a modification in GPCR expression or activation, as it has been proposed for P2Y12 expression in platelets of diabetic patients (Hu et al., 2017). However, the specific mechanism linking high glucose concentration to PI3Kγ activation needs further investigation.

Despite improvements in cardiovascular disease management, diabetic patients still present a higher risk of major thrombotic events and their recurrence compared to non-diabetic patients (Gao et al., 2015; Wilson et al., 2022). Glycemic control has long been considered as the main factor capable of limiting those risks (Diabetes et al., 2016; Stratton et al., 2000). Collectively, our work brings the evidence that hyperglycemia aggravates foam SMC formation through defective autophagy. Our results, together with data from literature, supporting the fact that hypoglycemic drugs could exert atheroprotective effects by promoting autophagy in SMCs, clearly demonstrate the importance of regulating this process in SMCs of diabetic patients, to avoid macrovascular complications (Chen et al., 2024; Xu et al., 2024). Moreover, our results shed light on the possibility of using of PI3K gamma inhibitors, which have passed safety clinical trials for the treatment of solid tumors, to prevent major cardiovascular events and potential recurrences in diabetic patients (Hong et al., 2023).

Figure legends

Figure 1: High glucose concentration leads to increased lipid accumulation in smooth muscle cells *in vitro* and *in vivo*: A: Summarized procedure to induce a hyperglycemic wire-injured atheromatous mouse model: LDLR$^{-/-}$ mice fed with Western diet during 9 weeks, received 5 injections of either streptozotocin (STZ, 50 mg/kg, n=8) or citrate buffer vehicle (0.1 N, Ctrl, n=9). 10 days after the last STZ injection, mice underwent a carotid artery injury and were euthanized 4 weeks after. Blood and injured carotid arteries were harvested for analysis. B: Representative images of carotid artery sections stained with Bodipy 493/503 (green, neutral lipids) and α-SMA (red, smooth muscle cells, SMCs). Internal elastic lamina autofluorescence appears in grey. Scale bar: 100 µm. C: Neutral lipids inside the lesion were quantified by measuring the Bodipy labeling inside the neointima. D: Lipid accumulation in SMCs was quantified based on the merged red/green labeling. E, F: Representative images of neutral lipid

accumulation (left) in human SMCs (hSMC, E) or murine SMCs (mSMC, F) incubated either in low (L, 1 g/L) or high (H, 5 g/L) glucose medium for 7 days, followed by oxLDL (oxL, 200 µg/mL) exposure for 3 additional days. Neutral lipids (NL) were stained using Nile red and nuclei using DAPI. Neutral lipid labeling was quantified using Image J software (right). Scale bar: 50 µm (n= 10 to 13). Data are represented as mean +/- SEM, of a fold increase compared with the low glucose with OxLDL condition (E, F). Statistical analysis was performed using Mann-Whitney (C, D) and Friedman tests (E, F). *p<0.05, **p<0.01, ***p<0.001, ****p<0.0001

Table 1: End point metabolic parameters of STZ and control LDLR$^{-/-}$ mice. Results are presented as the mean +/- SEM. Statistical analysis were performed using a Mann Whitney test (* p<0,05, ** p<0,01; *** p<0,001).

Figure 2: High glucose concentration induced SMC lipid accumulation is due to defective autophagy. SMCs were cultured as described in Figure 1 with or without OxLDL A: LC3 protein expression was assessed after cell incubation, with or without bafilomycin (Baf,100 nM) 6 hours before the end of the experiment (n=5). B: Autophagic flux of SMCs treated as described in A, calculated by subtracting the densitometry value of Baf-untreated LC3-II from corresponding Baf-treated LC3-II value (n=4). C: Representative confocal images (left) of low (L) and high (H) glucose concentration cultured hSMCs following transfection with the GFP-LC3-RFP-LC3ΔG plasmid as described in the Material and Methods. The GFP/RFP ratio (right), estimates the autophagic flux activity (n=4). Scale bar: 20 µm. D: mRNA expression analysis of ATG-5 and ATG-7 by RTq PCR (n=3). E-G: Foam cell formation in the presence of 200 µg/ml of oxLDL under various experimental conditions: E: Representative images of neutral lipids accumulation (left, green) of hSMCs transfected either with control (ctrl), ATG-5 or ATG-7 si-RNA and lipid labeling quantification (right) (n=4). F, G: Representative images of neutral lipid accumulation (left, green) of hSMCs treated with (+) or without (-) 3-methyladenine (3Ma, 20 µM, F) or rapamycin (Rp, 100 nM, G) and lipid labeling quantification (right) (n=6-7). DAPI was used to visualize the nuclei. Scale bars: 50 (D) and 70 µm (F, G). Results are presented as the mean +/- SEM, as a fold increase of the low glucose without the treatment (A-C, F, G) or low glucose with si-RNA control (D, E) conditions. Statistical analysis were performed using the Friedman test (A, D-G), Wilcoxon test (B), and unpaired t test (C). *p<0,05, **p<0,01.

Figure 3: PI3Kγ drives increased foam SMC formation induced by high glucose concentration. hSMC were cultured in oxLDL (OxL, 200 µg/ml) low (L) and high (H) glucose medium and then treated with the indicated treatment. A: Representative

images of neutral lipids accumulation (left, green) and quantification (right) of hSMCs cultured with (+) or without (-) LY294002 (10 µM). DAPI was used to visualized nuclei. (n=6) B: Images of neutral lipids accumulation (left, green) and quantification (right) of hSMCs treated under class I PI3K isoforms inhibitors A66 (10 µM), AZD-6482 (10 µM) or IPI-549 (1 µM). DAPI was used to visualized nuclei. (n=6 to 10). C: Quantification of the total cholesterol level and free cholesterol/cholesterol ester ratio in hSMCs incubated in the presence (+) or absence (-) of IPI-549. (n= 4 to 5) D: Cholesterol efflux to ApoA assessed in hSMCs cultured as described in C. (n=10) E, F: Representative images of neutral lipids accumulation (left, green) and quantification (right) in wild-type (WT) or PI3Kγ knockout (PI3KγKO) mSMCs treated as described in Figure 1. Nuclei were labeled using DAPI. (n=8) Scale bars: 50 µm. Results are presented as the mean +/- SEM and as a fold increase of the low glucose condition (A-D). Statistical analysis were performed using the Friedman test (A), unpaired t test (B-D), and Kruskal Wallis test (E). *p<0,05, **p<0,01, ***p<0,001.

Figure 4: Blocking PI3Kγ reverses high glucose-induced autophagy alterations. A: Confocal images (left) of LC3 staining in hSMCs cultured in high glucose (H) concentration treated with (+) or without (-) IPI-549 (1µM). LC3 puncta quantification (right) was performed using Image J software. Scale bar: 50 µm. (n=6) B: LAMP-1 and LC3 genic expression in hSMC stimulated with low (L) or high glucose (H) with (+) or without (-) IPI-549 (n=7). C: Confocal images (left) of LC3 staining in WT and PI3KγKO mSMCs cultured in low (L) or high glucose (H) medium. LC3 puncta quantification (right) was performed using Image J software. Scale bar: 50 µm. (n=6). D: Representative confocal images (left) of low (L) and high (H) glucose concentration cultured WT and PI3KγKO mSMCs following transfection with the GFP-LC3-RFP-LC3ΔG plasmid as described in the Material and Methods. Scale bar: 20 µm. The GFP/RFP ratio (right) was quantified using Image J software. E, F: LAMP-1 and LC3 genic expression in WT (E) and PI3Kγ KO (F) murine SMCs stimulated with low (L) or high (H) glucose medium (n=7 to 8). Results are presented as the mean +/- SEM, as a fold increase of low glucose condition. Statistical analysis were performed using Wilcoxon test (A, C-F) and Friedman test (B). *p<0,05, **p<0,01.

Figure 5: High glucose-impaired TFEB nuclear translocation mediating defective autophagy and foam cell formation, is reversed by PI3Kγ inhibition. A: Representative images of neutral lipids accumulation (left, green) of hSMCs transfected either with control (ctrl) or TFEB si-RNA and lipid labeling quantification (right). Nuclei were

visualized with DAPI staining. Scale bar: 50 µm. (n=4). B-D: mRNA expression analysis of TFEB (B), LAMP-1 (C) or LC3 (D) by RTq PCR (n=4). E, F: TFEB protein expression in the cytosolic (Cyto) and nuclear (Nucl) fractions of hSMCs cultured as described in Figure 1, using Western blot analysis (n=10) G: Phospho-Ser211 and total TFEB protein expression analysis in hSMCs stimulated as described in Figure 1 with (+) or without (-) IPI-549 (1µM), following Western Blot analysis (n=6). H: Ratio of TFEB protein expression in nuclear and cytoplasmic fractions from hSMCs treated the absence (-) or presence (+) of IPI-549 following western blot analysis (n=8). Results are presented as the mean +/- SEM, as a fold increase of the low glucose with (A-C) or without (D-G) the si-RNA control condition. Statistical analysis were performed using the Wilcoxon test (C-F, H) and Friedman test (A, B,G). *p<0,05, **p<0,01.

Anzinger, J.J., J. Chang, Q. Xu, M.K. Barthwal, T. Bohnacker, M.P. Wymann, and H.S. Kruth. 2012. Murine bone marrow-derived macrophages differentiated with GM-CSF become foam cells by PI3Kgamma-dependent fluid-phase pinocytosis of native LDL. *J Lipid Res*. 53:34-42.

Auge, N., F. Maupas-Schwalm, M. Elbaz, J.C. Thiers, A. Waysbort, S. Itohara, H.W. Krell, R. Salvayre, and A. Negre-Salvayre. 2004. Role for matrix metalloproteinase-2 in oxidized low-density lipoprotein-induced activation of the sphingomyelin/ceramide pathway and smooth muscle cell proliferation. *Circulation*. 110:571-578.

Basatemur, G.L., H.F. Jorgensen, M.C.H. Clarke, M.R. Bennett, and Z. Mallat. 2019. Vascular smooth muscle cells in atherosclerosis. *Nat Rev Cardiol*. 16:727-744.

Bashore, A.C., H. Yan, C. Xue, L.Y. Zhu, E. Kim, T. Mawson, J. Coronel, A. Chung, N. Sachs, S. Ho, L.S. Ross, M. Kissner, E. Passegue, R.C. Bauer, L. Maegdefessel, M. Li, and M.P. Reilly. 2024. High-Dimensional Single-Cell Multimodal Landscape of Human Carotid Atherosclerosis. *Arteriosclerosis, thrombosis, and vascular biology*. 44:930-945.

Bonaa, K.H., J. Mannsverk, R. Wiseth, L. Aaberge, Y. Myreng, O. Nygard, D.W. Nilsen, N.E. Klow, M. Uchto, T. Trovik, B. Bendz, S. Stavnes, R. Bjornerheim, A.I. Larsen, M. Slette, T. Steigen, O.J. Jakobsen, O. Bleie, E. Fossum, T.A. Hanssen, O. Dahl-Eriksen, I. Njolstad, K. Rasmussen, T. Wilsgaard, J.E. Nordrehaug, and N. Investigators. 2016. Drug-Eluting or Bare-Metal Stents for Coronary Artery Disease. *The New England journal of medicine*. 375:1242-1252.

Chang, J.D., G.K. Sukhova, P. Libby, E. Schvartz, A.H. Lichtenstein, S.J. Field, C. Kennedy, S. Madhavarapu, J. Luo, D. Wu, and L.C. Cantley. 2007. Deletion of the phosphoinositide 3-kinase p110gamma gene attenuates murine atherosclerosis. *Proceedings of the National Academy of Sciences of the United States of America*. 104:8077-8082.

Chen, K., H.J. Jin, Z.H. Wu, B.F. Zhang, J. Wu, Z.Y. Huang, Y.P. Huang, X.W. Lu, and X.T. Zheng. 2024. Glucagon-like peptide-1 receptor agonist exendin 4 ameliorates diabetes-associated vascular calcification by regulating mitophagy through the AMPK signaling pathway. *Mol Med*. 30:58.

Chen, Z., C. Ouyang, H. Zhang, Y. Gu, Y. Deng, C. Du, C. Cui, S. Li, W. Wang, W. Kong, J. Chen, J. Cai, and B. Geng. 2022. Vascular smooth muscle cell-derived

hydrogen sulfide promotes atherosclerotic plaque stability via TFEB (transcription factor EB)-mediated autophagy. *Autophagy*. 18:2270-2287.

Diabetes, C., I. Complications Trial /Epidemiology of Diabetes, and G. Complications Study Research. 2016. Intensive Diabetes Treatment and Cardiovascular Outcomes in Type 1 Diabetes: The DCCT/EDIC Study 30-Year Follow-up. *Diabetes Care*. 39:686-693.

Gao, L., S.J. Park, Y. Jang, S. Lee, C.J. Kim, Y. Minami, D. Ong, T. Soeda, R. Vergallo, H. Lee, B. Yu, S. Uemura, and I.K. Jang. 2015. Comparison of Neoatherosclerosis and Neovascularization Between Patients With and Without Diabetes: An Optical Coherence Tomography Study. *JACC Cardiovasc Interv*. 8:1044-1052.

Gistera, A., D.F.J. Ketelhuth, S.G. Malin, and G.K. Hansson. 2022. Animal Models of Atherosclerosis-Supportive Notes and Tricks of the Trade. *Circ Res*. 130:1869-1887.

Hirsch, E., V.L. Katanaev, C. Garlanda, O. Azzolino, L. Pirola, L. Silengo, S. Sozzani, A. Mantovani, F. Altruda, and M.P. Wymann. 2000. Central role for G protein-coupled phosphoinositide 3-kinase gamma in inflammation. *Science (New York, N.Y*. 287:1049-1053.

Hong, D.S., M. Postow, B. Chmielowski, R. Sullivan, A. Patnaik, E.E.W. Cohen, G. Shapiro, C. Steuer, M. Gutierrez, H. Yeckes-Rodin, R. Ilaria, B. O'Connell, J. Peng, G. Peng, N. Zizlsperger, A. Tolcher, and J.D. Wolchok. 2023. Eganelisib, a First-in-Class PI3Kgamma Inhibitor, in Patients with Advanced Solid Tumors: Results of the Phase 1/1b MARIO-1 Trial. *Clin Cancer Res*. 29:2210-2219.

Hu, L., L. Chang, Y. Zhang, L. Zhai, S. Zhang, Z. Qi, H. Yan, Y. Yan, X. Luo, S. Zhang, Y. Wang, S.P. Kunapuli, H. Ye, and Z. Ding. 2017. Platelets Express Activated P2Y(12) Receptor in Patients With Diabetes Mellitus. *Circulation*. 136:817-833.

Kaizuka, T., H. Morishita, Y. Hama, S. Tsukamoto, T. Matsui, Y. Toyota, A. Kodama, T. Ishihara, T. Mizushima, and N. Mizushima. 2016. An Autophagic Flux Probe that Releases an Internal Control. *Mol Cell*. 64:835-849.

Komaru, Y., T. Takeuchi, L. Suzuki, T. Asano, and K.Y. Urayama. 2020. Recurrent cardiovascular events in patients with newly diagnosed acute coronary syndrome: Influence of diabetes and its management with medication. *J Diabetes Complications*. 34:107511.

Liu, K., and M.J. Czaja. 2013. Regulation of lipid stores and metabolism by lipophagy. *Cell Death Differ*. 20:3-11.

Lupieri, A., N.F. Smirnova, R. Solinhac, N. Malet, M. Benamar, A. Saoudi, I. Santos-Zas, L. Zeboudj, H. Ait-Oufella, E. Hirsch, P. Ohayon, T. Lhermusier, D. Carrie, J.F. Arnal, D. Ramel, S. Gayral, and M. Laffargue. 2020. Smooth muscle cells-derived CXCL10 prevents endothelial healing through PI3Kgamma-dependent T cells response. *Cardiovascular research*. 116:438-449.

Michael, D.R., T.S. Davies, L. Laubertova, H. Gallagher, and D.P. Ramji. 2015. The phosphoinositide 3-kinase signaling pathway is involved in the control of modified low-density lipoprotein uptake by human macrophages. *Lipids*. 50:253-260.

Mocci, G., K. Sukhavasi, T. Ord, S. Bankier, P. Singha, U.T. Arasu, O.O. Agbabiaje, P. Makinen, L. Ma, C.J. Hodonsky, R. Aherrahrou, L. Muhl, J. Liu, S. Gustafsson, B. Byandelger, Y. Wang, S. Koplev, U. Lendahl, G.K. Owens, N.J. Leeper, G. Pasterkamp, M. Vanlandewijck, T. Michoel, A. Ruusalepp, K. Hao, S. Yla-Herttuala, M. Vali, H. Jarve, M. Mokry, M. Civelek, C.J. Miller, J.C. Kovacic, M.U. Kaikkonen, C. Betsholtz, and J.L.M. Bjorkegren. 2024. Single-Cell Gene-Regulatory Networks of Advanced Symptomatic Atherosclerosis. *Circulation research*. 134:1405-1423.

Mosquera, J.V., G. Auguste, D. Wong, A.W. Turner, C.J. Hodonsky, A.C. Alvarez-Yela, Y. Song, Q. Cheng, C.L. Lino Cardenas, K. Theofilatos, M. Bos, M. Kavousi, P.A. Peyser, M. Mayr, J.C. Kovacic, J.L.M. Bjorkegren, R. Malhotra, P.T. Stukenberg, A.V. Finn, S.W. van der Laan, C. Zang, N.C. Sheffield, and C.L. Miller. 2023.

Integrative single-cell meta-analysis reveals disease-relevant vascular cell states and markers in human atherosclerosis. *Cell Rep*. 42:113380.
Napolitano, G., and A. Ballabio. 2016. TFEB at a glance. *J Cell Sci*. 129:2475-2481.
Osborne, J.C., Jr. 1986. Delipidation of plasma lipoproteins. *Methods Enzymol*. 128:213-222.
Pi, S., L. Mao, J. Chen, H. Shi, Y. Liu, X. Guo, Y. Li, L. Zhou, H. He, C. Yu, J. Liu, Y. Dang, Y. Xia, Q. He, H. Jin, Y. Li, Y. Hu, Y. Miao, Z. Yue, and B. Hu. 2021. The P2RY12 receptor promotes VSMC-derived foam cell formation by inhibiting autophagy in advanced atherosclerosis. *Autophagy*. 17:980-1000.
Poznyak, A., A.V. Grechko, P. Poggio, V.A. Myasoedova, V. Alfieri, and A.N. Orekhov. 2020. The Diabetes Mellitus-Atherosclerosis Connection: The Role of Lipid and Glucose Metabolism and Chronic Inflammation. *Int J Mol Sci*. 21.
Ray, J.L., R. Leach, J.M. Herbert, and M. Benson. 2001. Isolation of vascular smooth muscle cells from a single murine aorta. *Methods Cell Sci*. 23:185-188.
Robichaud, S., A. Rasheed, A. Pietrangelo, A. Doyoung Kim, D.M. Boucher, C. Emerton, V. Vijithakumar, L. Gharibeh, G. Fairman, E. Mak, M.A. Nguyen, M. Geoffrion, R. Wirka, K.J. Rayner, and M. Ouimet. 2022. Autophagy Is Differentially Regulated in Leukocyte and Nonleukocyte Foam Cells During Atherosclerosis. *Circ Res*. 130:831-847.
Stratton, I.M., A.I. Adler, H.A. Neil, D.R. Matthews, S.E. Manley, C.A. Cull, D. Hadden, R.C. Turner, and R.R. Holman. 2000. Association of glycaemia with macrovascular and microvascular complications of type 2 diabetes (UKPDS 35): prospective observational study. *BMJ*. 321:405-412.
Swiader, A., H. Nahapetyan, J. Faccini, R. D'Angelo, E. Mucher, M. Elbaz, P. Boya, and C. Vindis. 2016. Mitophagy acts as a safeguard mechanism against human vascular smooth muscle cell apoptosis induced by atherogenic lipids. *Oncotarget*. 7:28821-28835.
Wilson, S., P. Mone, U. Kansakar, S.S. Jankauskas, K. Donkor, A. Adebayo, F. Varzideh, M. Eacobacci, J. Gambardella, A. Lombardi, and G. Santulli. 2022. Diabetes and restenosis. *Cardiovasc Diabetol*. 21:23.
Xi, G., X. Shen, C. Wai, M.F. White, and D.R. Clemmons. 2019. Hyperglycemia induces vascular smooth muscle cell dedifferentiation by suppressing insulin receptor substrate-1-mediated p53/KLF4 complex stabilization. *The Journal of biological chemistry*. 294:2407-2421.
Xu, H., J. Fu, Q. Tu, Q. Shuai, Y. Chen, F. Wu, and Z. Cao. 2024. The SGLT2 inhibitor empagliflozin attenuates atherosclerosis progression by inducing autophagy. *J Physiol Biochem*. 80:27-39.
Xue, J.H., Z. Yuan, Y. Wu, Y. Liu, Y. Zhao, W.P. Zhang, Y.L. Tian, W.M. Liu, Y. Liu, and C. Kishimoto. 2010. High glucose promotes intracellular lipid accumulation in vascular smooth muscle cells by impairing cholesterol influx and efflux balance. *Cardiovasc Res*. 86:141-150.
Zhao, Y., X. Jia, X. Yang, X. Bai, Y. Lu, L. Zhu, W. Cheng, M. Shu, Y. Zhu, X. Du, L. Wang, Y. Shu, Y. Song, and S. Jin. 2022. Deacetylation of Caveolin-1 by Sirt6 induces autophagy and retards high glucose-stimulated LDL transcytosis and atherosclerosis formation. *Metabolism*. 131:155162.

Acknowledgments

We thank the Phenotyping Department of the UMS006 CREFRE-Anexplo Platform and the GeT-Santé facility (I2MC, Inserm, Génome et Transcriptome, GenoToul, Toulouse, France) and TRI-Genotoul (light microscopy; member of the national

infrastructure France-Bioimaging Infrastructure supported by the French National Research Agency) for their technical support.

Funding

This work was funded in part by Inserm, Foundation for medical research (FRM, Target PI3K) and French Foundation (FDF cardiovascular: SMC and Diabetes), and the FEDER-région Occitanie program (INSPIRE). H.L. and I.M. were supported by a research grant from the University of Toulouse.

Data Availability Statement

Data will be made available upon reasonable request.

Conflicts of Interest

The authors declare no conflict of interest.

Figure 1: High glucose concentration leads to increased lipid accumulation in smooth muscle cells in vivo and in vitro

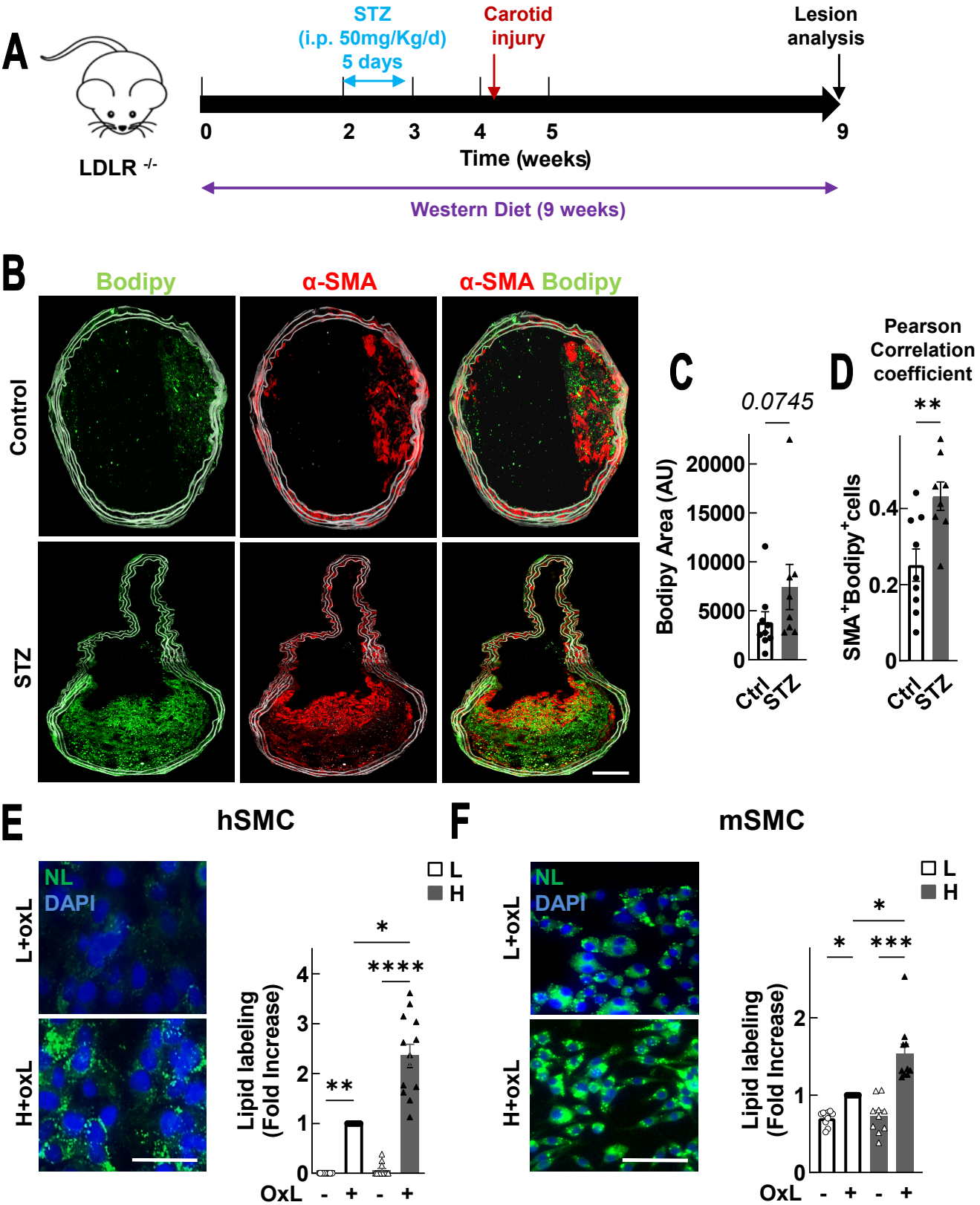

Table 1: End point plasmatic metabolic parameters of STZ and control LDLR -/- mice.

Parameter	Control	STZ
Body weight,g	*31,3±0,9*	*22,5±4,2****
Blood glucose D+7 post STZ, mg/dL	*173,6±9,7*	*325±40,9****
Blood glucose, mg/dL	*159,5±5,1*	*514,5±57,2****
Insulin, pg/dL	*1150,3±179,9*	*220,8±175,3***
Total cholesterol, mg/dL	*1346,9±133,4*	*2167,1±381,7*
LDL cholesterol, mg/dL	*485,6±43,6*	*944,9±204,5**
HDL cholestrol, mg/dL	*66,1±4,1*	*130,5±48,1*
LDL/HDL	*7,2±0,5*	*8,6±1,3*
Triglycerides, mg/dL	*534,5±54,2*	*1729,4±560,2**

Figure 2: High glucose concentration impairs autophagy and induced-SMC lipid accumulation

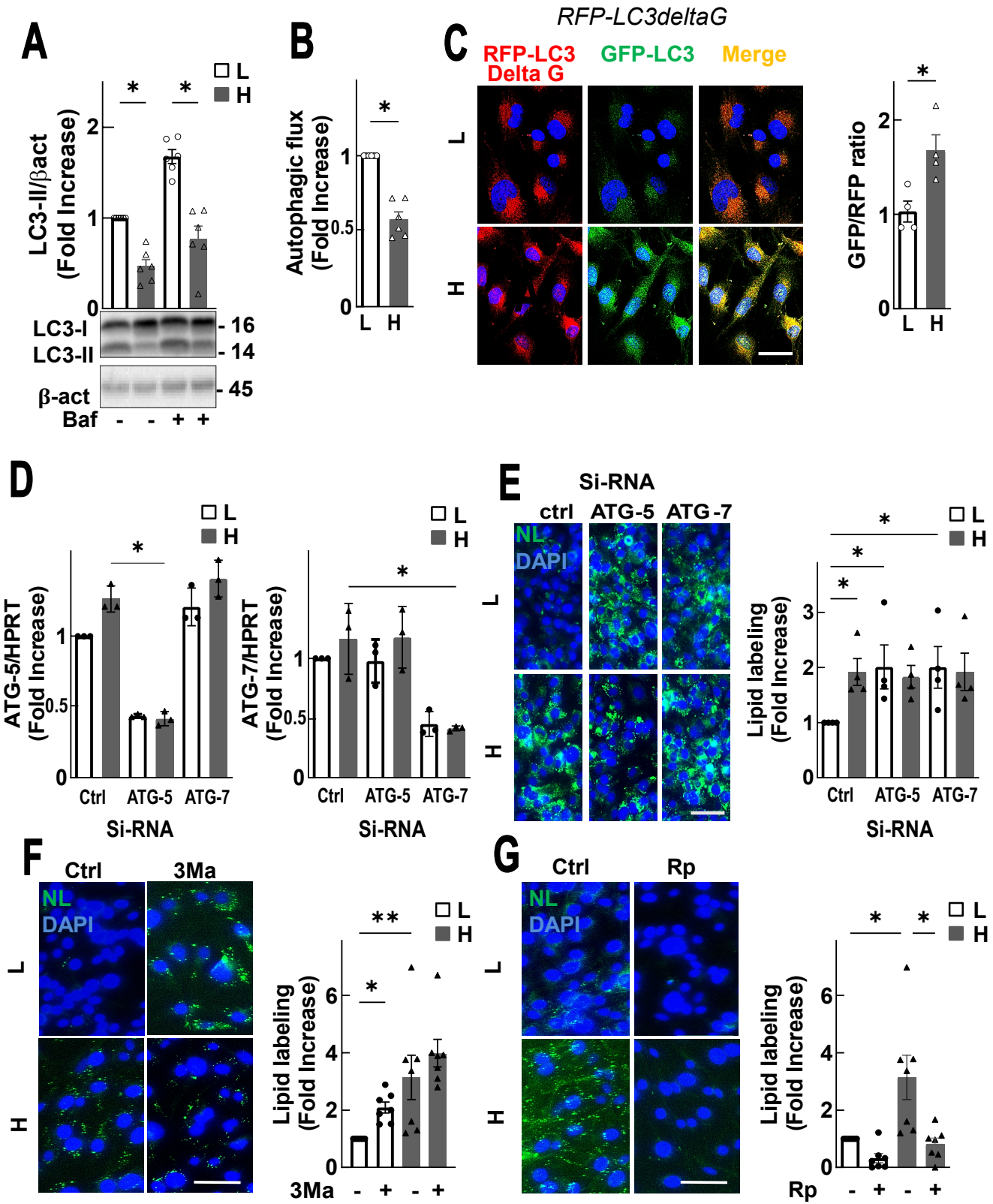

Figure 3: PI3Kγ drives increased foam SMC formation induced by high glucose concentration.

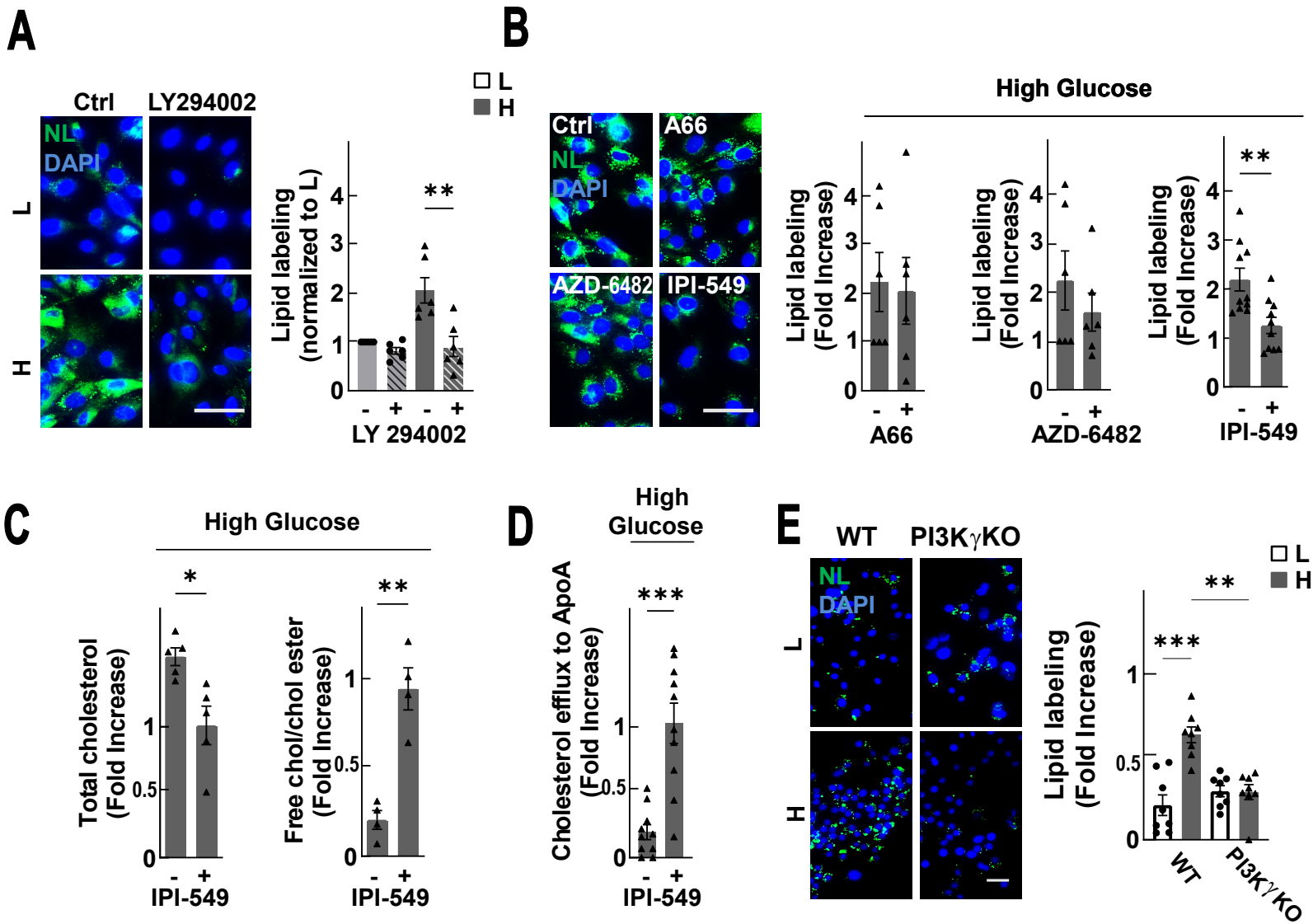

Figure 4 : Blocking PI3Kγ reverses high glucose-induced autophagy alterations

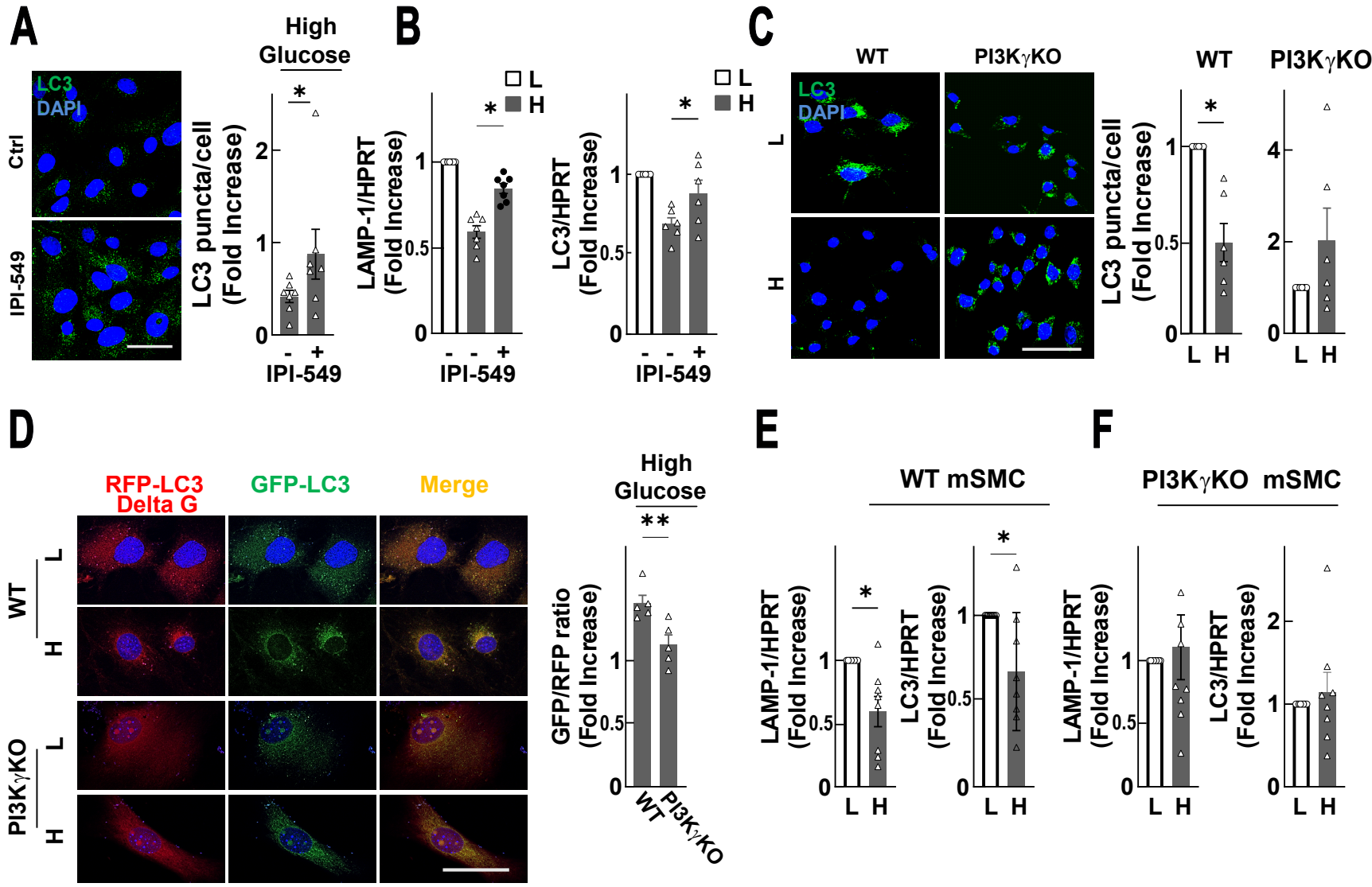
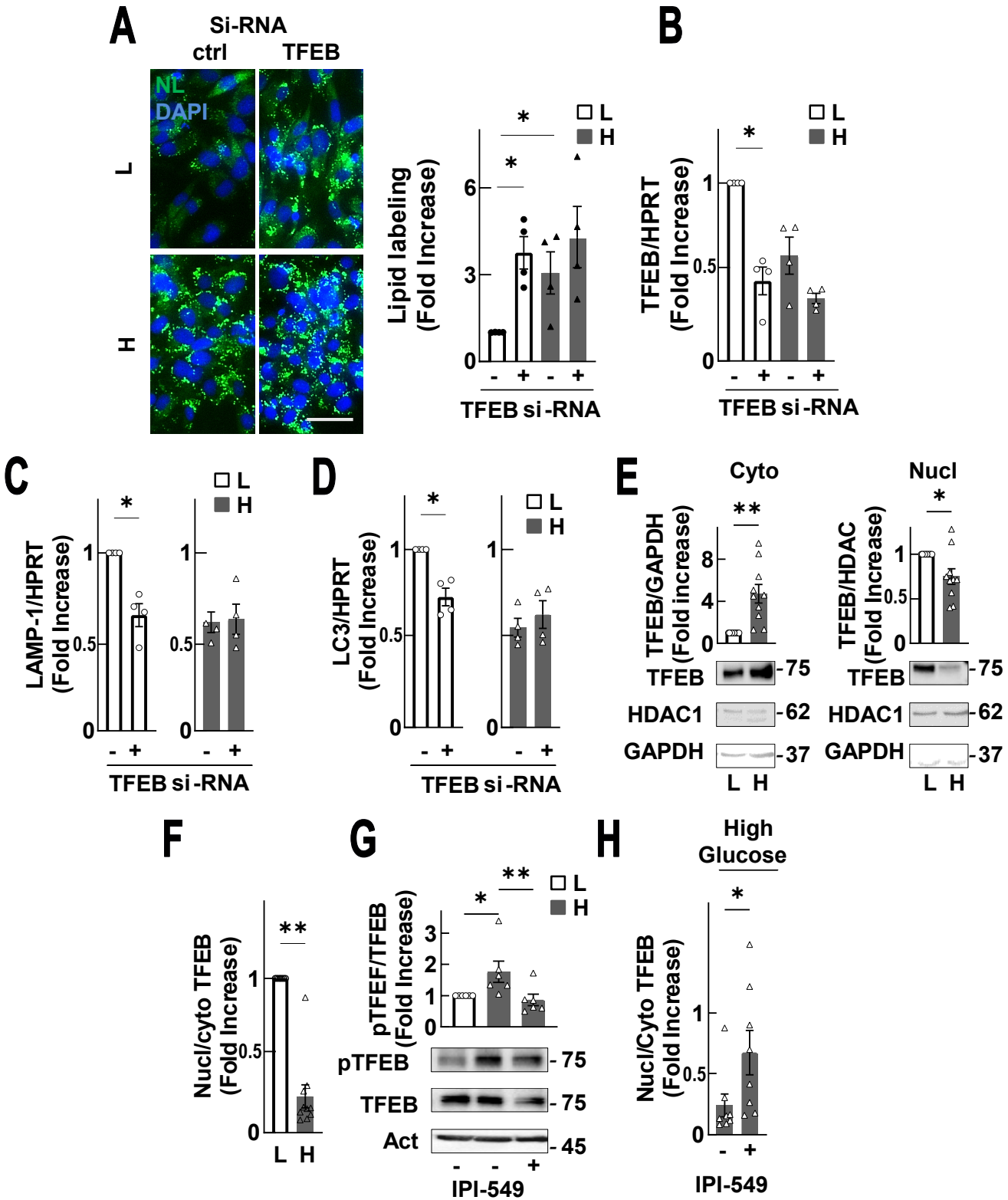
Figure 5: High glucose-impaired TFEB nuclear translocation mediating defective autophagy and foam cell formation, is reversed by PI3Kγ inhibition.